Energy 293 (2024) 130612

Contents lists available at ScienceDirect

Energy

journal homepage: www.elsevier.com/locate/energy

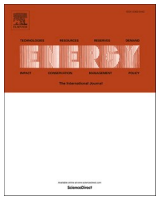

Thermal-hydraulic-structural analysis and optimization of supercritical CO_2 solar tower receiver

Yanjuan Wang [a], Yi Li [a], Zheng Zhu [a], Zhewen Chen [b,*], Jinliang Xu [a]

[a] The Beijing Key Laboratory of Multiphase Flow and Heat Transfer, North China Electric Power University, Beijing, 102206, China
[b] State Key Laboratory of Heavy Oil Processing, China University of Petroleum-Beijing, Beijing, 102249, China

ARTICLE INFO

Keywords:
Eccentric tube
High non-uniform heat flux
Multiphysics coupling
Supercritical CO_2 tubular receiver
Solar power tower

ABSTRACT

The supercritical CO_2 receiver in solar tower power plants withstands high temperature and large thermal stress caused by highly non-uniform solar radiation. The application of eccentric tube in solar power tower plants was innovatively proposed to solve this problem. A three-dimensional thermal-fluid-mechanical coupling model of complex eccentric tube structure with high non-uniform heat (NUH) flux was constructed. The results showed that the eccentric receiver was appropriate for non-uniform and half-perimeter uniform heat fluxes. The eccentric tube exhibited a considerable improvement in tube-wall refrigeration, reflected in the maximum temperature and stresses. The highly NUH flux distribution in the receiver proved to be the main factor causing plastic deformation. Moreover, the distribution of the temperature, stress, and generalized thermal deviation factor (*GTDF*) with eccentric distance were also determined—they all decreased with an increase in the eccentric distance. Consequently, the key operating parameters for the eccentric receiver performance were investigated. The maximum temperature of the eccentric receiver was greatly reduced by 46.6–109.1 K and the *GTDF* was effectively reduced by approximately 13.9–51.4% under all the simulated working conditions—indicating the eccentric receiver to be a superior candidate to the current cavity tubular receiver of solar power tower plants.

1. Introduction

Considering the intensification of pollutant emissions, the exhaustion of fossil fuels, and climate change, it has become essential to develop cleaner and more efficient power conversion systems. Concentrated solar power technology stands out amongst a variety of renewable energy resources, owing to its safety, high efficiency, and negligible greenhouse emissions [1]. Solar power towers are considered to be superior candidates for producing clean energy from concentrated solar power [2]. Compared to parabolic collectors and linear Fresnel reflectors, solar power towers can provide higher operating temperatures, and their design concept is highly flexible—that is, various heliostats, heat transfer fluids, and receivers can be chosen, affording access to improved efficiency and lower thermal energy storage costs [3,4].

Merchán et al. [5] summarized the state-of-the-art technology of solar tower receivers and their challenges. For example, to ensure high cycle efficiency, the temperature of the solar receiver can exceed 1000 K. Moreover, the solar receiver withstands high thermal gradients caused by highly non-uniform solar radiation concentrated by the heliostat field. These can lead to high thermal stress and the rupturing of the receiver tube, limiting the lifespan of the plant [6].

Consequently, much effort has been devoted to the design and optimization of receivers, as they are vital components linking the power cycle and heliostat field [7,8]. In practice, tubular receivers with molten salts as heat transfer fluids are the most frequently used receiver concepts [9]. Du et al. [10] studied the thermal stress and fracture of a molten salt receiver, their results showing that the minimum solar flux was merely 0.19 MW/m^2 lower than the average solar flux when fatigue damage appeared on the receiver tube, the damage being likely to occur under the current operating conditions, seriously affecting the safety of solar power tower plants. Consequently, higher working temperatures are being pursued to boost the cycle efficiency and reduce the cost of molten salt receivers [11]. However, molten salts decompose at temperatures greater than 600 °C [12]. Accordingly, the performance of supercritical CO_2 (sCO_2) tubular receivers has been widely investigated as they can withstand a higher heat flux [13], which translates to a more compact receiver with lower flow resistance but potentially higher cost [14].

* Corresponding author. College of Mechanical and Transportation Engineering, China University of Petroleum-Beijing, Beijing, 102206, China.
E-mail addresses: 90102184@ncepu.edu.cn (Y. Wang), liyidsg@gmail.com (Y. Li), zhuzheng1028@163.com (Z. Zhu), 2022880013@cup.edu.cn (Z. Chen), xjl@ncepu.edu.cn (J. Xu).

https://doi.org/10.1016/j.energy.2024.130612
Received 14 June 2023; Received in revised form 28 December 2023; Accepted 4 February 2024
Available online 5 February 2024

The key technical problems of high-temperature sCO_2 tubular receiver include the materials, geometric designs, and methods that boost heat flux absorptance, reduce heat loss, and provide better reliability at higher temperatures [14]. Several methods have been investigated for this purpose. One option is to enhance tube-wall refrigeration, which can reduce the thermal stress in the receiver. A high non-uniform heat flux (NUH) increases the stress and deformation of the sCO_2 receiver panel. Wang et al. [15] optimized the matching between the solar flux and flow arrangements of an sCO_2 receiver panel to improve the thermomechanical performance, with the ideal flow allocation exhibiting the smallest thermal loss and stress being determined using a matching factor of one.

Others have attempted to develop new receiver concepts or optimize geometric designs to boost the receiver reliability [16–18]. For example, when the center of the inner and outer walls of the tube are not concentric—that is, an eccentric tube—the resulting circumferential unevenness of the tube thickness can optimize the heat transfer with the NUH flux in the angular direction, showing potential to further reduce the temperature gradients of the receiver tube while maintaining the flow resistance [19]. Consequently, the eccentric tube offers an extra degree of freedom compared to a simple tube, which can be used to optimize the solar receiver, making the use of eccentric tubes in solar power tower receivers worth considering. Pérez-álvarez et al. [20] proposed an eccentric bayonet tube with molten salt as the heat transfer fluid, which used the asymmetry of the flow channel to enhance heat transfer in the angular direction where the heat flux was high. This could increase the convective heat transfer, although the flow resistance was significantly higher than that in simple tubes. Wang et al. [21] analyzed the performance of an eccentric tube receiver in parabolic trough collectors. They found that the thermal stress decreased with eccentricity, but the mechanical stress increased. They ignored the increase in mechanical stress, which may become dominant owing to the low heat flux in the parabolic trough collectors. Consequently, the damage decreased with increasing wall thickness, whereas it first increased before decreasing under a high heat flux because of the combined effect of the thermal and mechanical stresses [22]. Because the solar flux is much higher in solar power tower plants, it is essential to investigate the application of eccentric tubes in solar power tower plants.

While solar power tower receiver has been widely explored in the literature, limited studies discussed the application of eccentric tube in solar power tower plants with highly heat flux and few models to manage the complex geometry with detailed structural analysis. To our knowledge, this study represents the inaugural attempt to discuss the application of eccentric tube in solar power tower plants with highly heat flux. The primary contributions are encapsulated as follows:

(1) The application of eccentric tube in solar power tower plants with highly heat flux was firstly discussed. The thermomechanical behaviors of the eccentric and conventional tubular receivers were compared, to examine the potential advantages and disadvantages of using an eccentric receiver in a solar power tower receiver.
(2) A detailed three-dimensional thermal-fluid-mechanical coupling model of a complex geometry was developed. The influence of eccentricity on the comprehensive performance of an eccentric solar power tower receiver was studied.
(3) The influence of key working parameters—such as heat flux distribution, mass flux, and inlet temperature—on the comprehensive performance of the eccentric receiver, were investigated. The conditions were representative of the common working conditions of a receiver, where solar irradiation is highly non-uniform.

2. Methods: Numerical model

2.1. Physical model

A cavity tubular receiver typically comprises an aperture, several auxiliary surfaces, and receiver panels consisting of vertical tubes that absorb the heat flux from heliostats [23]. Considering the similarity of the heat flux on each tube, a single 1-m tube was selected as the physical model to simplify the calculation. Accordingly [15], a basic tube (Fig. 1) and an eccentric tube (Fig. 2) with an outer and inner diameter of 35 and 20 mm, respectively, were considered as the physical models. The real operating conditions—that is, a mass sCO_2 flow rate of 0.4 kg/s, working pressure of 20 MPa, inlet temperature of 773.15 K, and a Gaussian-shaped NUH flux of maximum value 412.1 kW/m^2—were selected for calculation.

An eccentric tube can be achieved when the centers of the outer and inner tubes of the basic receiver tube are not concentric. The distance between the center of the inner and outer tube can be defined as the eccentric distance (e_c) (Fig. 2). This modification distributes the circumferential tube thickness to match the circumferential high NUH flux. A thinner wall can be coupled with a higher heat flux. With an increase in e_c, the wall facing the solar irradiation becomes thinner. To ensure tube safety, the largest e_c can be considered [24], taking into account the influences of the working pressure, temperature, and metal properties.

As the solar flux is unevenly distributed on the tubular receiver's outer wall, the receiver tube is semi-circumferentially heated and can be divided into front (absorbing solar flux) and back (adiabatic) sides (Fig. 1(c)). The outer front side is loaded with a Gaussian-shaped NUH flux [4], calculated as follows:

$$q = q_{\max} \cdot f(x,z) \tag{1}$$

$$f(x,z) = \exp\left\{ -3 \times \left[\frac{x^2 + (z-0.5)^2}{\chi^2} \right] \right\} \tag{2}$$

where $q_{\max}$ denotes the maximum heat flux, χ being 0.9. Fig. 3 shows a typical Gaussian-shaped NUH flux, which is non-uniform in both the x- and z-directions.

Owing to the high temperature, pressure and NUH flux, Inconel 625 steel was selected [15,25]. The thermophysical properties of the samples are shown in Fig. 4. The sCO_2 properties with respect to temperature and pressure were obtained using REFPROP [26].

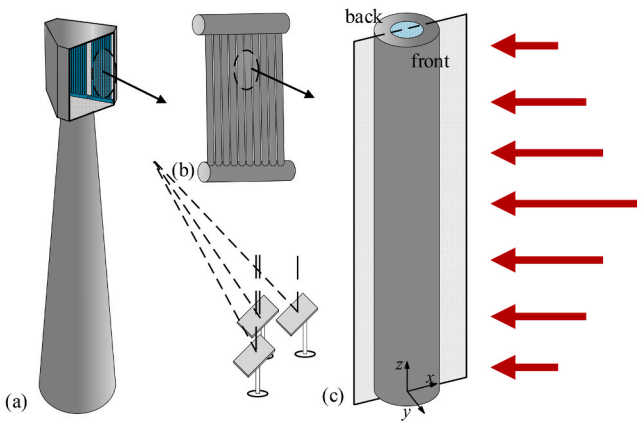

(a) Solar tower (b) Tube row for the tubular receiver (c) basic receiver tube.

Fig. 1. Schematic diagram of the receiver tube in a solar tower.

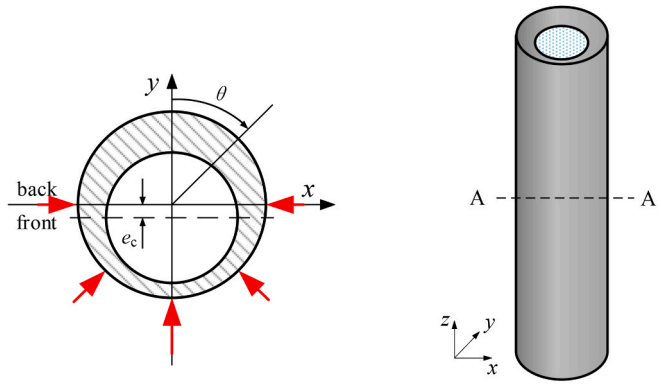

(a) Construction process of the novel structure (b) 3D structure

Fig. 2. Physical configuration of the eccentric tube.

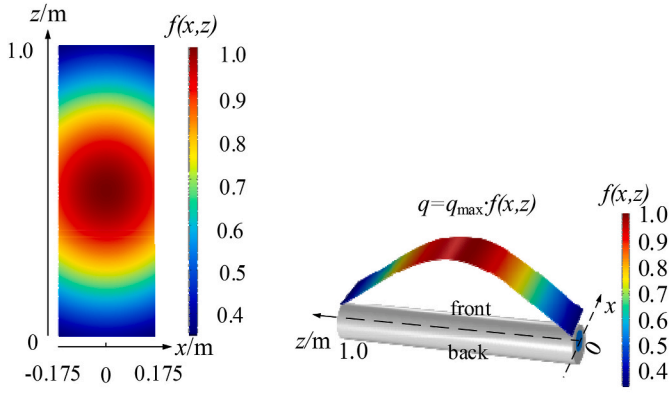

(a) On a panel. (b) Outer front side.

Fig. 3. The NUH flux distribution.

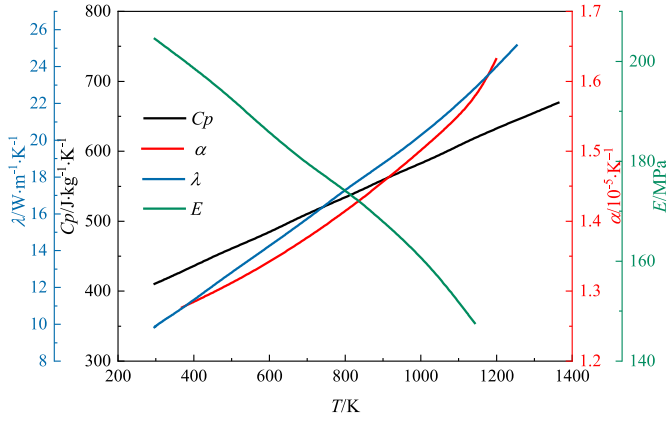

Fig. 4. Physical properties of Inconel 625 at atmospheric pressure.

2.2. Governing equations and boundary conditions

In this study, a three-dimensional steady-state receiver tube model with coupled hydrodynamics, thermodynamics, and solid mechanics was developed. The basic equations for thermodynamic analysis comprise the mass, energy, and momentum conservation equations [27–29]. The Re number of the sCO_2 is much higher than 3.5×10^5, indicating turbulent flow, so the k–ε turbulent model with the wall function [30] can be adopted to describe the process of sCO_2 flow and heat transfer in the receiver.

To determine the mechanical characteristics of the solar receiver, both the temperature distribution (T) from the thermodynamic simulation and the pressure load between the inner and outer walls can be used. The equivalent stress is a combination of the thermal stress caused by the temperature gradient and structural stress caused by the pressure load. The thermal stress obeys the following equations [31]:

$$\sigma_{r,\mathrm{t}} = \frac{\alpha E \Delta T}{2(1-\nu)\ln\left(\frac{r_o}{r_i}\right)}\left[-\ln\frac{r_o}{r} - \frac{r_i^2}{r_o^2-r_i^2}\left(1-\frac{r_o^2}{r^2}\right)\ln\left(\frac{r_o}{r_i}\right)\right] \tag{3}$$

$$\sigma_{\theta,\mathrm{t}} = \frac{\alpha E \Delta T}{2(1-\nu)\ln\left(\frac{r_o}{r_i}\right)}\left[1-\ln\frac{r_o}{r} - \frac{r_i^2}{r_o^2-r_i^2}\left(1+\frac{r_o^2}{r^2}\right)\ln\left(\frac{r_o}{r_i}\right)\right] \tag{4}$$

$$\sigma_{l,\mathrm{t}} = \frac{\alpha E \Delta T}{2(1-\nu)\ln\left(\frac{r_o}{r_i}\right)}\left[1-2\ln\frac{r_o}{r} - \frac{2r_i^2}{r_o^2-r_i^2}\ln\left(\frac{r_o}{r_i}\right)\right] \tag{5}$$

The mechanical stress equations are as follows [32]:

$$\sigma_{r,\mathrm{p}} = \frac{p_i r_i^2}{r_o^2-r_i^2}\left(1-\frac{r_o^2}{r^2}\right) \tag{6}$$

$$\sigma_{\theta,\mathrm{p}} = \frac{p_i r_i^2}{r_o^2-r_i^2}\left(1+\frac{r_o^2}{r^2}\right) \tag{7}$$

$$\sigma_{l,\mathrm{p}} = \frac{p_i r_i^2}{r_o^2-r_i^2} \tag{8}$$

The equivalent stress is calculated using the von Mises theory [22]:

$$\sigma_{\mathrm{eq}} = \sqrt{\frac{(\sigma_r-\sigma_\theta)^2+(\sigma_\theta-\sigma_l)^2+(\sigma_l-\sigma_r)^2}{2}} \tag{9}$$

The detailed boundary conditions are shown in Fig. 5.

Note that both convection and radiation were considered on the receiver's outer surface, depicted as follows:

$$q_{\mathrm{conv}} = h_{\mathrm{o}}(T_{\mathrm{o}} - T_{\mathrm{a}}) \tag{10}$$

$$h_{\mathrm{o}} = 0.557\cdot 10^{-6}\left(\frac{T_{\mathrm{o}}-T_{\mathrm{a}}}{l}\right)^{0.25} \tag{11}$$

$$q_{\mathrm{rad}} = \varepsilon\sigma_{\mathrm{S-B}}\left(T_{\mathrm{o}} - T_{\mathrm{sky}}\right) \tag{12}$$

where h_{o} is the natural convective heat transfer coefficient [32], $\varepsilon = 0.87$ is the emissivity of the receiver tube [33], and $\sigma_{\mathrm{S\text{-}B}}$ is the Stefan Boltzmann constant (5.67×10^{-8} W•m^{-2} K^{-4}). T_{a} (the ambient temperature) and T_{sky} (the effective sky temperature) are defined as 298.15 and 290.15 K, respectively [34].

The generalized thermal deviation factor (*GTDF*) [35] has been shown to be an accurate and convenient criterion for evaluating whether plastic or elastic deformation occurs on the tube wall under mechanical and thermal stress loading. It can be defined as follows:

$$\begin{cases} GTDF = \dfrac{\sqrt{(M+T-T_{\mathrm{ave}})^2+3M^2N^2}}{T_{\mathrm{s}}}, \\ M = \dfrac{Pr_i^2}{\alpha E\left(r_o^2-r_i^2\right)},\ N = \dfrac{r_o^2}{r_i^2},\ T_{\mathrm{s}} = \dfrac{\sigma_{\mathrm{s}}}{\alpha E} \end{cases} \tag{14}$$

where T_{ave} denotes the average temperature, and T_{s} denotes a feature temperature of the yield strength σ_{s}. The *GTDF* is a nondimensional parameter used to estimate the ratio of the equivalent stress to the yield stress (σ_{s}). It responds, to a certain extent, to the magnitude of the equivalent stress. When the $GTDF > 1$, the equivalent stress is larger than σ_{s}—that is plastic deformation occurs. When the $GTDF < 1$, elastic

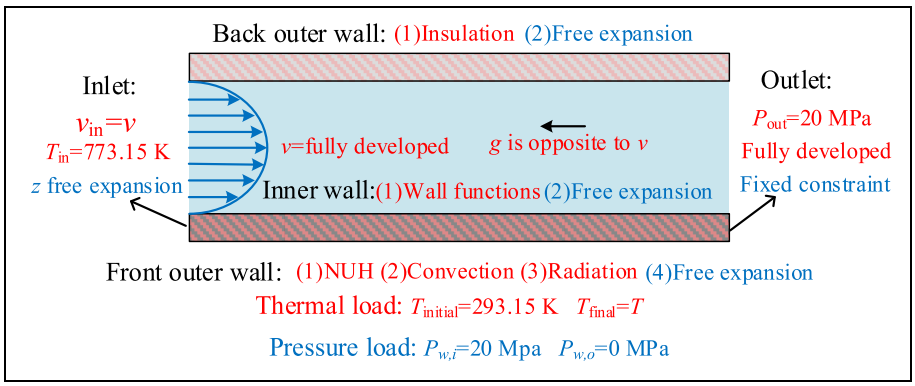

Fig. 5. Detailed boundary conditions.

deformation occurs. Hence, in practical applications, a *GTDF* < 1 is required in most regions of the tube to avoid stress failure.

2.3. Model validations

The sCO_2 turbulence experimental data under high temperatures, pressures, and heat fluxes are limited. Consequently, the experimental results of Zhu et al. [36] were selected to validate the thermodynamic model, its pressure and heat flux reaching 20.6 MPa and 200 kW/m^2, respectively. The detailed experimental conditions are shown in Fig. 6. As shown in Fig. 6, the average fluid temperature agrees well with the experimental results, with a maximum relative error of 2.8%. The relative error of the inner receiver wall temperature is 1%, confirming the accuracy of the thermodynamic model.

As it was challenging to measure the stress in the receiver tube with the high heat flux, the mechanical model was verified using a theoretical method [37]. The radial temperature and pressure difference between the inner and outer wall were 93.15 K and 20 MPa, respectively. The other parameters were the same as those under the standard conditions (Fig. 6). In Fig. 7, the theoretical results of the thermal (Eqs. (3), (4) and (5)) and mechanical stresses (Eqs. (6), (7) and (8)) are consistent with the numerical results, proving the feasibility of the proposed multi-physical model.

3. Results and discussions

3.1. Effect of eccentric distance and heat flux distribution

A high NUH flux can be a challenging problem in sCO_2 receiver

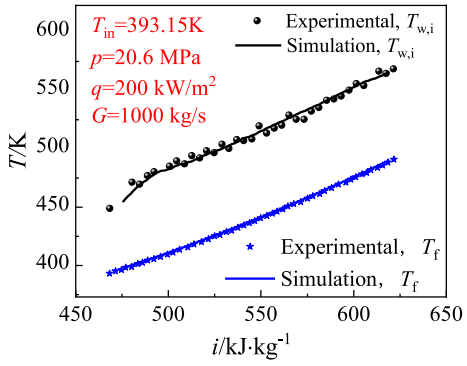

Fig. 6. Comparisons between simulation and experimental results. (Tube length = 2 m, D = 14 mm, d = 10 mm, tube material is 1Cr18Ni9Ti, the tube is uniformly heated by direct current heating via a copper braid wire. The outer wall is adiabatic because it is wrapped with aluminum silicate heat-insulating cotton. Inlet temperature = 393.15 K, mass flow = 1000 kg m^{-2} s^{-1}, and inlet pressure = 20.6 MPa).

design, and reducing its negative effects has been the subject of many studies [38–42]. In this section, the effect of heat flux distribution on the performance of both traditional and eccentric tubes is examined. Three common heat flux distributions—that is, the real operating condition (NUH), half-perimeter uniform heat flux, and uniform heat flux—were chosen, and the total heat flux of each case is equal.

Fig. 8 shows the influence of e_c and the heat flux distribution on the temperature distribution. Because the heat flux is applied directly to the outer surface of the receiver, T_{max} appears there. The temperature variation is analogous to that of the corresponding heat flux distribution. T_{max} occurs when the maximum heat flux is located under non-uniform heating, whereas T_{max} appears at the outlet under uniform and half-perimeter uniform heat fluxes. T_{max} under the NUH flux is 1165.5 K, which is approximately 5.8% and 19.0% higher than that of the semi-perimeter uniform and uniform heat flux cases, respectively. In Fig. 9, T_{max} decreases with an increase in e_c for the non-uniform and half-perimeter uniform cases, whereas it increases for the uniform case. Compared with the conventional receiver it decreases by 78.6 K (approximately 6.7%) and 64.9 K (approximately 5.8%), respectively, for the non-uniform and half-perimeter uniform cases when e_c is 3.2 mm. Consequently, the eccentric receiver can effectively reduce T_{max} for non-uniform and half-perimeter uniform cases.

Figs. 10 and 11 show the influence of e_c and the heat flux distribution on the stress distribution. The thermal stress is approximately six times greater than mechanical stress and is dominated under a high heat flux under all simulated working conditions. Consequently, the variation in the equivalent stress is analogous to that of the thermal stress. The maximum equivalent stress occurs in the tube outer wall for the non-uniform and half-perimeter uniform cases, whereas it is located in the inner tube wall for the uniform case. The maximum equivalent stress is 383.9, 367.6, and 246.6 MPa, respectively, for the non-uniform, half-perimeter uniform, and uniform cases, when e_c is 0 mm. The maximum thermal and equivalent stresses for the uneven heat flux distributions are considerably higher than those for the uniform heat flux distribution. Uneven heat flux distribution causes serious thermal stress, making it essential to mitigate this effect.

The equivalent stress and thermal stress decrease with an increase in e_c for the non-uniform and half-perimeter uniform cases. Compared to the conventional receiver, the equivalent stress is reduced by 58.69 and 72.37 MPa, respectively, for the non-uniform and half-perimeter uniform cases. Consequently, an eccentric tube can effectively reduce the maximum temperature, thermal stress, and equivalent stress. Furthermore, the flow resistance remains almost the same as the flow channel remains unchanged.

Fig. 12 shows the effects of e_c and the heat flux distribution on the *GTDF*. As is evident, no plastic deformation occurs for the uniform heat flux case, whereas plastic deformation occurs for the non-uniform and half-perimeter uniform cases, a high NUH flux distribution being the main factor causing plastic deformation. The eccentric tube structure

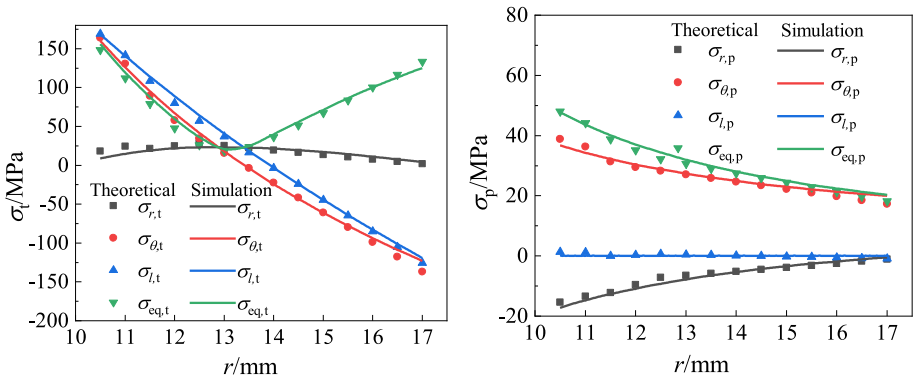

(a) Thermal stress (b) Mechanical stress

Fig. 7. Validation of structural model against theoretical results.

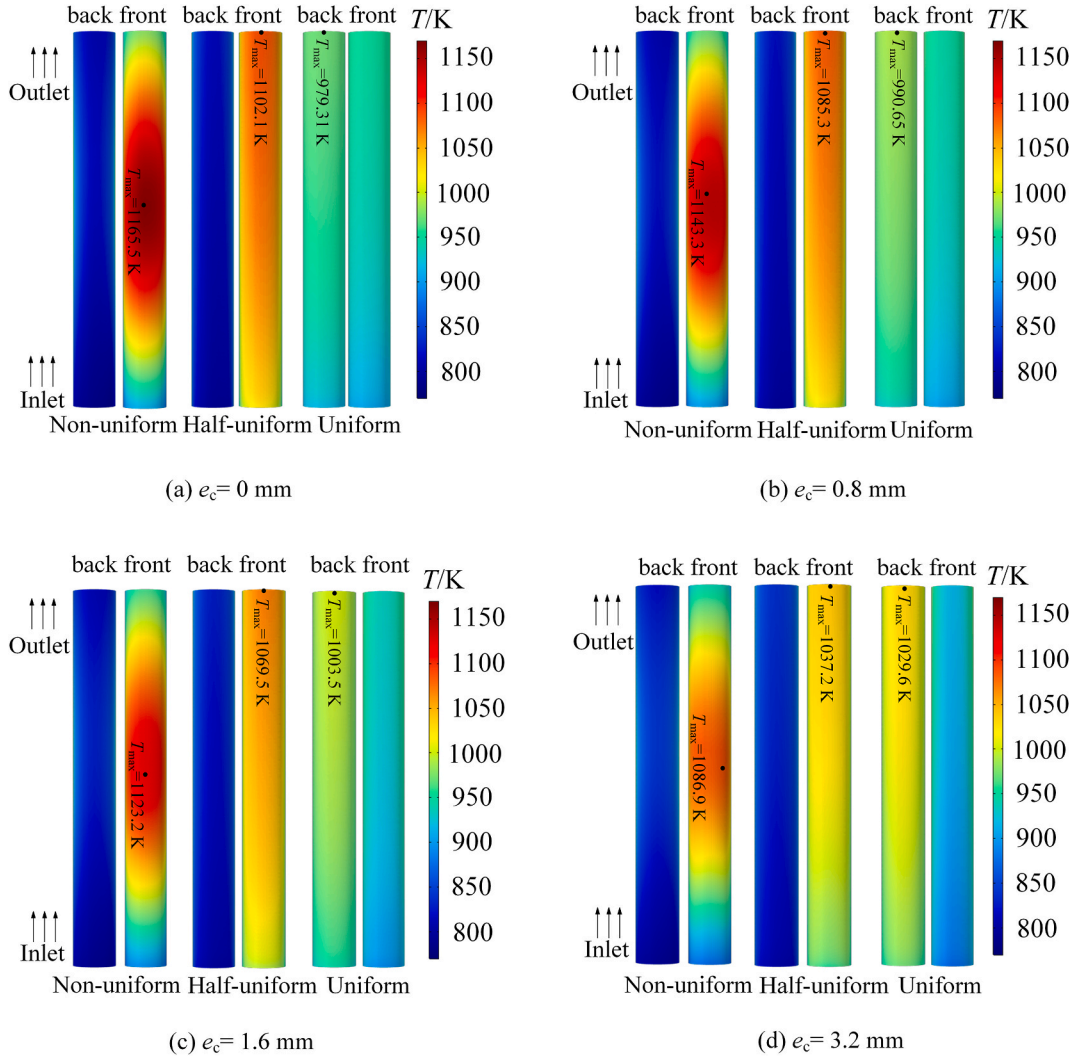

(a) e_c= 0 mm (b) e_c= 0.8 mm

(c) e_c= 1.6 mm (d) e_c= 3.2 mm

Fig. 8. Temperature distribution with e_c and heat flux distribution.

can effectively reduce the *GTDF*, the *GTDF* decreasing with an increase in e_c under the non-uniform and half-perimeter uniform cases. The maximum *GTDF* of the outer wall decreases from 4.32 to 2.79 to 2.32 (46.29%) and 1.67 (40.14%), respectively, for the non-uniform and half-perimeter uniform cases, indicating that the eccentric tube structure can greatly reduce the risk of plastic deformation of the receiver under non-uniform and half-perimeter uniform cases. This further proves the applicability of the eccentric tube in solar power tower receivers.

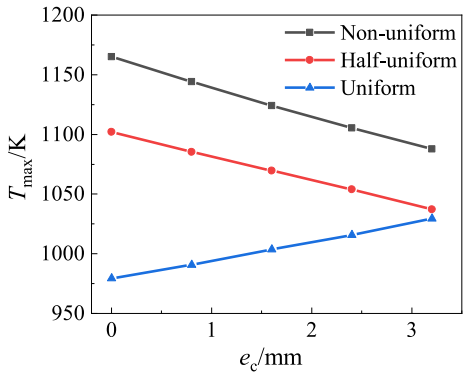

Fig. 9. Variation of T_{max} with heat flux distribution and e_c.

3.2. Effects of the mass flux, heat flux, and inlet temperature

Figs. 13–15 show the key working parameters—that is, the mass flux, heat flux, and inlet temperature, on the performance of the eccentric tube under the mass flux in the range of 0.2–0.6 kg/s, the average heat flux (q_{ave}) of 200–400 kW/m^2 and the inlet temperature of 573.15–973.15 K.

As is evident, plastic deformation occurs in the solar power tower receiver owing to the high NUH flux. The eccentric receiver effectively reduces the maximum temperature and plastic deformation under all simulated working conditions. In particular, when the NUH flux is high, as shown in Fig. 14, the *GTDF* and T_{max} increase rapidly with an increase in the NUH flux for the traditional receiver. The eccentric receiver greatly reduces the *GTDF* and T_{max}, and the reduction in the *GTDF* and T_{max} increases with the NUH flux. When q_{ave} is in the 200–400 kW/m^2 range, the *GTDF* increases from 1.9 to 9.4 and T_{max} increases from 1042.1 to 1278.5 K for a traditional tube. When e_c is 3.2 mm, the *GTDF* and T_{max} decrease by 0.5–4.0 (approximately 26.3–42.5%) and 57.9–93.1 K (approximately 5.56–7.28%), respectively, compared with a traditional tube under all the simulated working conditions. This is beneficial for protecting the receiver and increasing its lifespan.

The maximum temperature of the eccentric receiver is greatly reduced by 46.6–109.1 K and the *GTDF* is effectively reduced by approximately 13.9–51.4% under all the simulated working conditions. This indicates the superiority of the eccentric receiver over the conventional receiver.

4. Conclusions

In this study, the application of an eccentric tube in solar power tower plants was firstly discussed. The thermal, fluid and mechanical performance of the complex eccentric receiver structures with a highly NUH flux were numerically investigated. The comprehensive performance of the eccentric receiver behavior including the temperature, stress, pressure drop, and the *GTDF* was obtained. The key working parameters—that is, the heat flux distribution, eccentric distance, inlet temperature and mass flux—were examined. The main conclusions drawn can be summarized as follows:

1) No plastic deformation occurred in the uniform heat flux case, whereas plastic deformation occurred in the non-uniform and half-perimeter uniform cases under typical working conditions. The maximum equivalent stress of the NUH flux case increased by 137.3 MPa compared with the uniform heat flux case in the conventional receiver. The highly NUH flux distribution in the receiver was the main factor causing plastic deformation.
2) The distributions of the temperature, stress, and *GTDF* with the eccentric distance were obtained. They all decreased with an increase in the eccentric distance. The eccentric receiver effectively reduced the maximum temperature and plastic deformation under all simulated working conditions.
3) The effects of the vital operating parameters on the performance of the eccentric receiver were investigated. The maximum temperature of the eccentric receiver was greatly reduced by 46.6–109.1 K and the *GTDF* was effectively reduced by approximately 13.9–51.4% under all the simulated working conditions the indicating the applicability of the eccentric tube in solar power tower receiver.

The eccentric receiver can be a superior candidate to the current

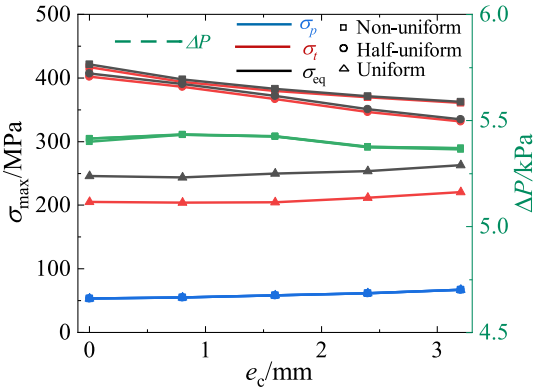

Fig. 11. Influence of heat flux distribution and e_c on σ_{max} at z = 0.5 mm and ΔP.

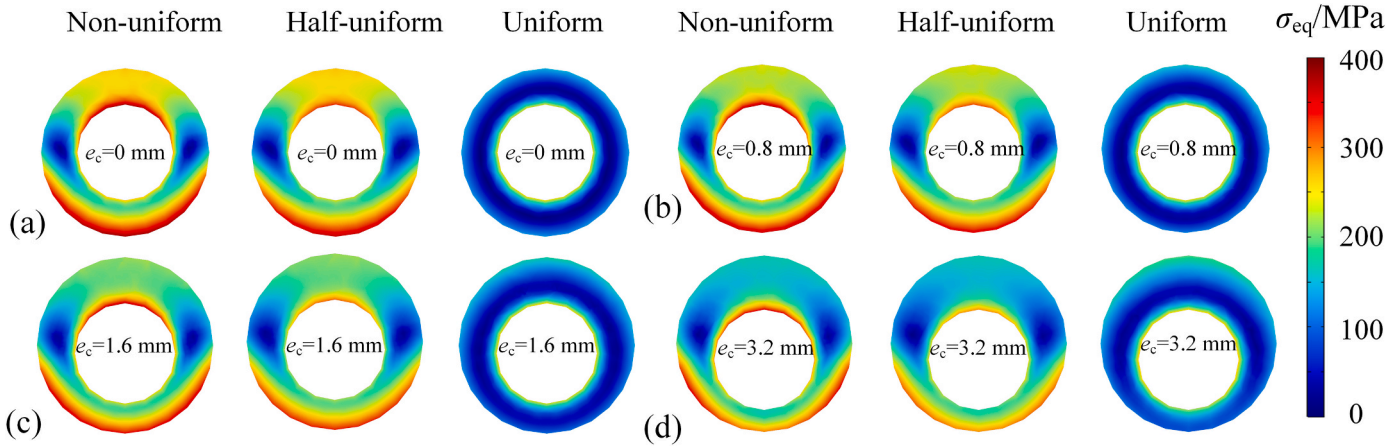

Fig. 10. Equivalent stress profiles at z = 0.5 m.

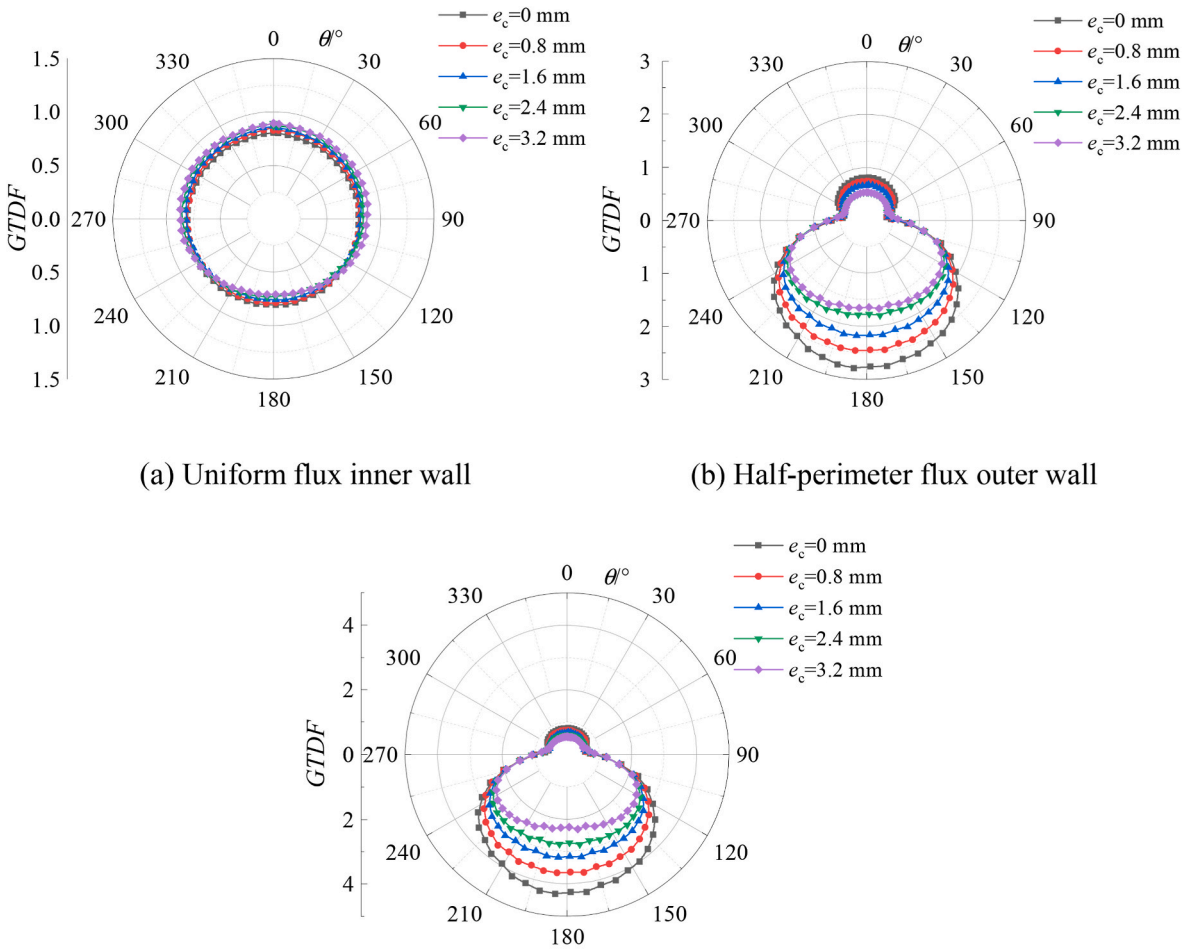

Fig. 12. The *GTDF* profiles with heat fluxes at $z = 0.5$ m.

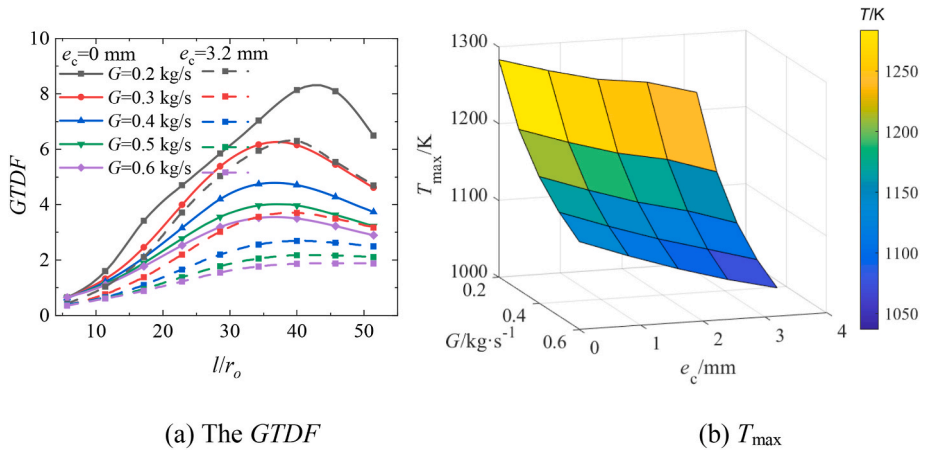

Fig. 13. Influence of the mass flux on the outer wall GTDF and T_{max} at $z = 0.5$ m (Inlet temperature = 773.15 K, q_{ave} = 300 kg/m^2, and working pressure = 20 MPa).

cavity tubular receiver of solar power tower plants. The research can provide theoretical support for the development of sCO_2 solar towers for industrial applications.

CRediT authorship contribution statement

Yanjuan Wang: Conceptualization, Funding acquisition, Investigation, Project administration, Resources, Writing – original draft, Writing – review & editing. **Yi Li:** Data curation, Formal analysis, Methodology, Software, Validation, Visualization, Writing – original draft, Writing –

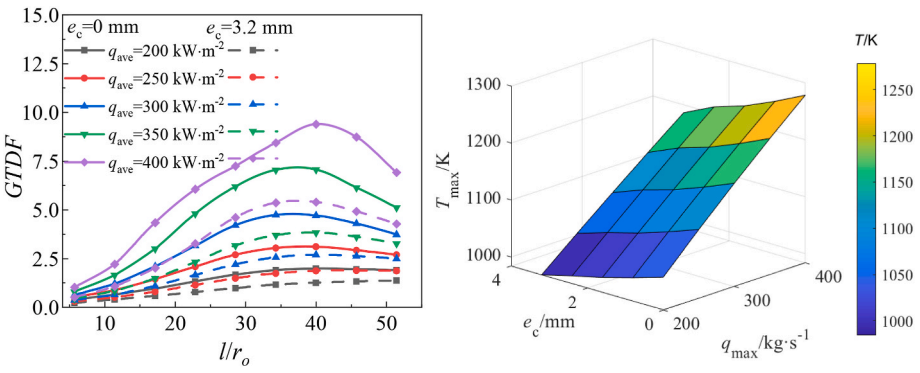

(a) The *GTDF* (b) T_{max}

Fig. 14. Influence of heat flux on the outer wall *GTDF* and T_{max} at $z = 0.5$ m (Inlet temperature = 773.15 K, mass flow = 0.4 kg/s, and working pressure = 20 MPa).

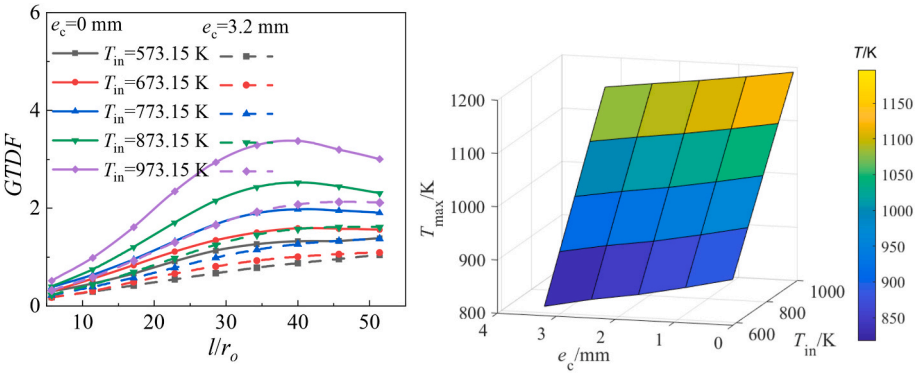

(a) The *GTDF* (b) T_{max}

Fig. 15. Influence of T_{in} on the outer wall *GTDF* and T_{max} at $z = 0.5$ m (Mass flow = 0.4 kg/s, q_{ave} = 300 kW/m^2, and working pressure = 20 MPa).

review & editing. **Zheng Zhu:** Investigation, Software, Writing – review & editing. **Zhewen Chen:** Conceptualization, Project administration, Resources, Supervision. **Jinliang Xu:** Funding acquisition, Resources, Supervision.

Declaration of competing interest

The authors declare that they have no known competing financial interests or personal relationships that could have appeared to influence the work reported in this paper.

Data availability

The data that has been used is confidential.

Acknowledgments

The authors appreciate the financial support provided by the National Natural Science Foundation of China (52076075 and 52130608).

Nomenclature

Cp	specific heat, J·kg^{-1}·K^{-1}
d	tube inner diameter, mm
D	tube outer diameter, mm
e_c	eccentric distance, mm
E	elastic modulus, MPa
g	gravity, m·s^{-2}
h	convective heat transfer coefficient, W·m^{-2}·K^{-1}
G	mass flux, kg·s^{-1}
GTDF	generalized thermal deviation factor
i	enthalpy, kJ·kg-1
l	tube length, m
NUH	non-uniform heat
P	working pressure, MPa
Δ*P*	pressure drop, kPa
q	heat flux, kW·m^{-2}
r	tube radius, mm
T	temperature, K
v	velocity, m·s^{-1}

Greek symbols

α	thermal expansion coefficient, K^{-1}
λ	thermal conductivity, W·m^{-1}·K^{-1}
θ	angle, °
ε	surface emissivity
υ	poisson's ratio
χ	standard deviation
σ_{eq}	equivalent stress, MPa
σ_p	mechanical stress, MPa
σ_s	yield strength, MPa
$\sigma_{S\text{-}B}$	Stefan Boltzmann constant, W·m^{-2}·K^{-4}
σ_t	thermal stress, MPa

Subscripts

a	ambient

ave	average
conv	convective heat transfer
eq	equivalent
f	fluid
i	inner
in	inlet
max	maximum
o	outer
out	outlet
p	pressure
rad	radiation heat transfer
r, θ, l	radial, tangential and axial direction
s	specific temperature
S–B	Stefan Boltzmann
t	thermal
w	tube wall

References

[1] IEA. Renewables 2022. Paris: IEA; 2022. https://www.iea.org/reports/renewables-2022.
[2] van der Hoeven M. Technology roadmap solar thermal electricity. Technical Report 2014;52.
[3] Zhang H, Baeyens J, Degrève J, Cacères G. Concentrated solar power plants: review and design methodology. Renewable and Sustainable Energy Reviews 2013;22:466–81.
[4] Wang K, Li M, Guo J, Li P, Liu Z. A systematic comparison of different S-CO2 Brayton cycle layouts based on multi-objective optimization for applications in solar power tower plants. Applied Energy 2018;212:109–21.
[5] Merchán RP, Santos MJ, Medina A, Calvo Hernández A. High temperature central tower plants for concentrated solar power: 2021 overview. Renewable and Sustainable Energy Reviews 2022;155:111828.
[6] Rodríguez-Sánchez MR, Soria-Verdugo A, Almendros-Ibáñez JA, Acosta-Iborra A, Santana D. Thermal design guidelines of solar power towers. Applied Thermal Engineering 2014;63(1):428–38.
[7] Conroy T, Collins MN, Grimes R. A review of steady-state thermal and mechanical modelling on tubular solar receivers. Renewable and Sustainable Energy Reviews 2020;119:109591.
[8] López-Herraiz M, Fernández AB, Martinez N, Gallas M. Effect of the optical properties of the coating of a concentrated solar power central receiver on its thermal efficiency. Solar Energy Materials and Solar Cells 2017;159:66–72.
[9] Yang J, Yang Z, Duan Y. Off-design performance of a supercritical CO2 Brayton cycle integrated with a solar power tower system. Energy 2020;201:117676.
[10] Du B, He Y, Zheng Z, Cheng Z. Analysis of thermal stress and fatigue fracture for the solar tower molten salt receiver. Applied Thermal Engineering 2016;99:741–50.
[11] Mancini TR, Gary JA, Kolb GJ, Ho CK. Power tower technology Roadmap and cost reduction plan. United States2011. p. Medium: ED; Size: 38 p..
[12] Iverson BD, Conboy TM, Pasch JJ, Kruizenga AM. Supercritical CO2 Brayton cycles for solar-thermal energy. Applied Energy 2013;111:957–70.
[13] Nithyanandam K, Pitchumani R. Thermal and structural investigation of tubular supercritical carbon dioxide power tower receivers. Solar Energy 2016;135:374–85.
[14] Ho CK, Iverson BD. Review of high-temperature central receiver designs for concentrating solar power. Renewable and Sustainable Energy Reviews 2014;29:835–46.
[15] Wang K, Jia P, Zhang Y, Zhang Z, Wang T, Min C. Thermal-fluid-mechanical analysis of tubular solar receiver panels using supercritical CO2 as heat transfer fluid under non-uniform solar flux distribution. Solar Energy 2021;223:72–86.
[16] Rodríguez-Sánchez MR, Laporte-Azcué M, Montoya A, Hernández-Jiménez F. Non-conventional tube shapes for lifetime extend of solar external receivers. Renewable Energy 2022;186:535–46.
[17] Qaisrani MA, Wei J, Fang J, Jin Y, Wan Z, Khalid M. Heat losses and thermal stresses of an external cylindrical water/steam solar tower receiver. Applied Thermal Engineering 2019;163:114241.
[18] Boerema N, Morrison G, Taylor R, Rosengarten G. High temperature solar thermal central-receiver billboard design. Solar Energy 2013;97:356–68.
[19] Wang Y, Gao S, Jiang Q, Li Y, Liu Q, Xu J. A new structure of cooling wall tube for supercritical CO2 Coal-Fired power plants. Journal of Thermal Science 2023;32(3):1239–50.
[20] Pérez-Álvarez R, Marugán-Cruz C, Santana D, Acosta-Iborra A. Influence of eccentricity on the thermomechanical performance of a bayonet tube of a central solar receiver. Applied Thermal Engineering 2023;223:119988.
[21] Wang F, Shuai Y, Yuan Y, Yang G, Tan H. Thermal stress analysis of eccentric tube receiver using concentrated solar radiation. Solar Energy 2010;84(10):1809–15.
[22] Chen Y, Zhang Y, Wang D, Hu S, Huang X. Effects of design parameters on fatigue–creep damage of tubular supercritical carbon dioxide power tower receivers. Renewable Energy 2021;176:520–32.
[23] Deng Q, Xiao X, Hao Y, Wang Q, Hu T, Wang Y. Heat transfer performance evaluation of a large-size cavity receiver in the solar power tower plant based on angle factors. Solar Energy 2017;148:78–86.
[24] Meyer JE, Vilminot KA, Frey J. ASME Piping Code: B31.1, power Piping. Online Companion Guide to the ASME Boiler and pressure Vessel Codes: Criteria and Commentary on Select Aspects of the Boiler & pressure Vessel Codes. ASME Press; 2020. p. 0.
[25] Upitis E, Moen RA, Carpenter ML, Newell Jr W, Grubb JF, Sutherlin RC, et al. Part 2, section II—materials and Specifications. Online Companion Guide to the ASME Boiler and pressure Vessel Codes: Criteria and Commentary on Select Aspects of the Boiler & pressure Vessel Codes. ASME Press; 2020. p. 0.
[26] Khalesi J, Sarunac N. Numerical analysis of flow and conjugate heat transfer for supercritical CO2 and liquid sodium in square microchannels. International Journal of Heat and Mass Transfer 2019;132:1187–99.
[27] Wang Y, Liu Q, Lei J, Jin H. Performance analysis of a parabolic trough solar collector with non-uniform solar flux conditions. International Journal of Heat and Mass Transfer 2015;82:236–49.
[28] Menter FR. Two-equation eddy-viscosity turbulence models for engineering applications. AIAA journal 1994;32(8):1598–605.
[29] Jones WP, Launder BE. The prediction of laminarization with a two-equation model of turbulence. International Journal of Heat and Mass Transfer 1972;15(2):301–14.
[30] Wang Y, Yu B, Gao S, Liu Q, Xu J. Performance analysis of cooling wall of supercritical CO2 coal-fired plants. Journal of Thermal Science 2022;31(6):1881–90.
[31] Barber JR. Elasticity. Springer; 2002.
[32] Segal A, Epstein M. Comparative performances of 'TOWER-TOP' and 'TOWER-REFLECTOR' central solar receivers. Solar Energy 1999;65(4):207–26.
[33] Gentile G, Picotti G, Binotti M, Cholette ME, Manzolini G. Dynamic thermal analysis and creep-fatigue lifetime assessment of solar tower external receivers. Solar Energy 2022;247:408–31.
[34] Forristall R. Heat transfer analysis and modeling of a parabolic trough solar receiver implemented in engineering equation solver. Golden, CO.(US): National Renewable Energy Lab.; 2003.
[35] Li X, Li G, Tang G, Fan Y, Yang D. A generalized thermal deviation factor to evaluate the comprehensive stress of tubes under non-uniform heating. Energy 2023;263:125710.
[36] Zhu B, Xu J, Wu X, Xie J, Li M. Supercritical "boiling" number, a new parameter to distinguish two regimes of carbon dioxide heat transfer in tubes. International Journal of Thermal Sciences 2019;136:254–66.
[37] Li X, Tang G, Yang D, Fan Y, Xu J. Thermal-hydraulic-structural evaluation of S–CO2 cooling wall tubes: a thermal stress evaluating criterion and optimization. International Journal of Thermal Sciences 2021;170:107161.
[38] Yang M, Yang X, Yang X, Ding J. Heat transfer enhancement and performance of the molten salt receiver of a solar power tower. Applied Energy 2010;87(9):2808–11.
[39] Lu J, Sheng X, Ding J, Yang J. Transition and turbulent convective heat transfer of molten salt in spirally grooved tube. Experimental Thermal and Fluid Science 2013;47:180–5.
[40] Wang K, He Y, Li P, Li M, Tao W. Multi-objective optimization of the solar absorptivity distribution inside a cavity solar receiver for solar power towers. Solar Energy 2017;158:247–58.
[41] Du B, Qiu Y, He Y, Xue X. Study on heat transfer and stress characteristics of the pressurized volumetric receiver in solar power tower system. Applied thermal engineering 2018;133:341–50.
[42] Wang K, He Y, Xue X, Du B. Multi-objective optimization of the aiming strategy for the solar power tower with a cavity receiver by using the non-dominated sorting genetic algorithm. Applied Energy 2017;205:399–416.